PCCP

PAPER

View Article Online
View Journal | View Issue

Cite this: *Phys. Chem. Chem. Phys.*, 2017, **19**, 29146

Ultrafast excited-state dynamics of 2,4-dimethylpyrrole†

Dongyuan Yang,[ab] Zhichao Chen,[a] Zhigang He,[a] Hengding Wang,[ab] Yanjun Min,[ab] Kaijun Yuan,[a] Dongxu Dai,[ac] Guorong Wu *[ac] and Xueming Yang[ac]

Received 14th September 2017,
Accepted 23rd October 2017

DOI: 10.1039/c7cp06292c

rsc.li/pccp

The ultrafast excited-state dynamics of 2,4-dimethylpyrrole following excitation at wavelengths in the range of 255.8–199.7 nm are studied using the time-resolved photoelectron imaging method. It is found that excitation at longer wavelengths (255.8, 250.0, 246.0 and 242.0 nm) results in population of the $S_1(^1\pi\sigma^*)$ state, which decays out of the photoionization window in less than 30 fs. At 237.7 nm, the second $^1\pi\sigma^*$ state is excited, which decays in about 130 fs. At shorter pump wavelengths (231.8, 224.8, 217.5 and 199.7 nm), the assignments are less clear-cut. We tentatively assign the initially photoexcited states to the $^1\pi3p$ Rydberg states, which decay in about 60 fs, with internal conversion to the $S_1(^1\pi\sigma^*)$ state as one of the decay channels. The lifetimes of these $^1\pi3p$ Rydberg states vary little with the pump wavelengths in this wavelength range.

I Introduction

Small heteroaromatic molecules offer experimentally and computationally tractable models for the understanding of the photochemistry and photophysics of a range of important biomolecules, including aromatic amino acids and DNA bases.[1–6] Such molecules usually have vanishingly small fluorescence quantum yields of strongly UV absorbing singlet states of $^1\pi\pi^*$ character, implying the existence of highly efficient radiationless decay mechanisms for these electronically excited states. Domcke and coworkers proposed a general mechanism for non-radiative decay in heteroaromatics, in which the singlet states of $^1\pi(3s/\sigma^*)$ character play a central role.[1,2] Pyrrole represents one of the prototypical molecules among these heteroaromatics and has been the subject of intensive experimental and theoretical studies.[7–26] In previous studies, we investigated the excited-state nonadiabatic dynamics of pyrrole and one of its methyl substituted derivatives, *N*-methylpyrrole (NMP), following excitation in the near UV region of its absorption spectrum, with one of the goals to study the methyl substitution effects.[21,22] For both molecules, the experimental and theoretical results were rationalized within the framework proposed by Domcke and coworkers and the role of the lowest-lying $^1\pi(3s/\sigma^*)$ state ($A_2(^1\pi\sigma^*)$ state for pyrrole and NMP) in the non-radiative decay of the excited states was also confirmed. Depending on the vibrational excitation of the $A_2(^1\pi\sigma^*)$ state of NMP, it has a lifetime about one to three orders of magnitude longer than that of pyrrole. In a later work by Blancafort *et al.*,[23] this drastic difference was explained to be due to an increased barrier along the C–N dissociation coordinate and an alternative decay mechanism was proposed, in which the $A_2(^1\pi\sigma^*)$ state of NMP with lower vibrational excitation decays to a lower-lying triplet state by intersystem crossing, followed by C–N bond dissociation. Here, we continue our efforts on this topic and investigate the excited-state nonadiabatic dynamics of another pyrrole methylated derivative with the C_{2v} symmetry broken, 2,4-dimethylpyrrole (2,4-DMP). The motivations are similar to those behind the study on NMP.[22] Besides studying the excited-state nonadiabatic dynamics of 2,4-DMP following excitation in the deep UV region, we also try to understand the methyl substitution effects on the excited-state nonadiabatic dynamics of pyrrole, which may aid the development of simple models of such dynamics extendable to larger molecules.

There are no previous studies on the UV absorption spectrum of 2,4-DMP. The main features of the UV absorption spectrum, as shown in Fig. 1, are very similar to those of pyrrole and analogous assignments can be made. As suggested by a reinterpretation of the electronic spectrum of pyrrole by Neville and Worth,[17] the broad, strong absorption band between 200–240 nm should be dominated by transitions to the $^1\pi3p$ Rydberg states, most of which gain intensities by vibronic coupling with the higher-lying $^1\pi\pi^*$ states. The strongly electric dipole-allowed transitions to the $^1\pi\pi^*$ states should only

[a] State Key Laboratory of Molecular Reaction Dynamics, Dalian Institute of Chemical Physics, 457 Zhongshan Road, Dalian 116023, Liaoning, China. E-mail: wugr@dicp.ac.cn
[b] University of Chinese Academy of Sciences, Beijing 100049, China
[c] Synergetic Innovation Center of Quantum Information & Quantum Physics, University of Science and Technology of China, Hefei, Anhui 230026, China

† Electronic supplementary information (ESI) available: Analysis of the photoelectron angular distributions at shorter pump wavelengths. See DOI: 10.1039/c7cp06292c

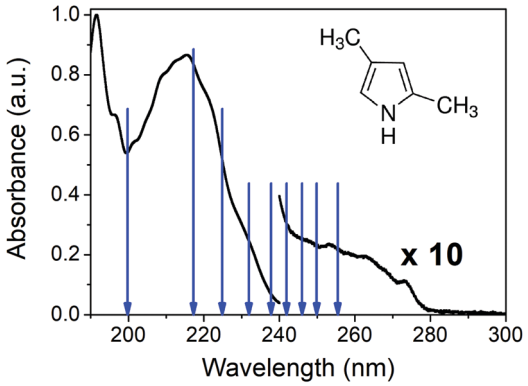

Fig. 1 The UV absorption spectrum of 2,4-DMP. The blue arrows indicate the pump wavelengths used in the current experiment.

become dominating at even shorter wavelengths. From 240 nm to longer wavelengths, there is a weak, broad band which should be due to the transition to the $^1\pi\sigma^*$ states. In pyrrole, the transitions from the ground state to the two $^1\pi\sigma^*$ states, $1^1\pi\sigma^*(A_2, S_1) \leftarrow 1^1\pi\pi(A_1, S_0)$ and $2^1\pi\sigma^*(B_1, S_1) \leftarrow 1^1\pi\pi(A_1, S_0)$, are electric dipole-forbidden, but gain intensity by vibronic coupling with the higher-lying $^1\pi\pi^*$ states. For 2,4-DMP, the symmetry is reduced (C_{2v} for pyrrole and C_s for 2,4-DMP) and these two transitions become electric dipole (weakly)-allowed. The corresponding absorption band is still very weak compared to that at 200–240 nm, but much stronger than that for pyrrole.

Ashfold and co-workers studied the photodissociation dynamics of 2,4-DMP excited to the $S_1(^1\pi\sigma^*)$ state using a combination of H (Rydberg) atom photofragment translational spectroscopy and *ab initio* electronic structure calculations.[13] Very similar photodissociation dynamics were observed to those for pyrrole. Stavros and coworkers further studied the dynamics of photo-excited 2,4-DMP using time-resolved velocity map imaging spectroscopy over the wavelength range of 276–238 nm.[16] Two dominant H atom elimination channels were inferred from the total kinetic energy release spectra and time-resolved total H-atom product yields, one which occurs with a time constant of ~120 fs producing H atoms with high kinetic energies centered around 5000–7000 cm^{-1} and a second channel with a time constant of ~3.5 ps producing H atoms with low kinetic energies centered around 2500–3000 cm^{-1}. The first of these channels was attributed to direct excitation from the S_0 state to the dissociative $S_1(^1\pi\sigma^*)$ state, followed by subsequent N–H bond fission. The time constant is invariant with the photo-excitation wavelength. The origins of the second channel are less clear-cut and the authors suggested that it is a consequence of populating higher-lying electronic states, for example the $S_2(^1\pi\sigma^*)$ state, followed by vibronic coupling into lower-lying intermediary states (S_1 or S_0), leading to prompt N–H bond fission.

In this paper, we present a time-resolved photoelectron imaging (TRPEI) study of the excited-state nonadiabatic dynamics of 2,4-DMP over a much-extended pump wavelength range of 255.8–199.7 nm. It is found that excitation at longer wavelengths (255.8, 250.0, 246.0 and 242.0 nm) results in excitation of the $S_1(^1\pi\sigma^*)$ state, which decays out of the photoionization window in less than 30 fs. At 237.7 nm, the second $^1\pi\sigma^*$ state is excited, which decays in ~130 fs. At shorter pump wavelengths (231.8, 224.8, 217.5 and 199.7 nm), the excitations are tentatively assigned to the transitions to the $^1\pi3p$ Rydberg states, which decay in about 60 fs. In Section II, we describe the experimental method used. In Section III, the analysis of the experimental data and detailed discussion of the excited state dynamics of 2,4-DMP are given. In Section IV, short conclusions are provided.

II Experimental

The experiment was carried out on a velocity map imaging (VMI) spectrometer, which is described elsewhere.[27] Nine different pump wavelengths in the range of 199.7–255.8 nm were used and the probe wavelength was fixed at 286.5 nm (1.8–2.2 μJ per pulse). Femtosecond laser pulses were obtained from a fully integrated Ti:Sapphire oscillator/regenerative amplifier system (<50 fs, 800 nm, 3.8 mJ and 1 kHz, Coherent, Libra-HE). Two optical parametric amplifiers with UV wavelength extension packages (OPA, Coherent, OperA Solo) were used, each pumped by a fraction of the amplifier output (1.3 mJ per pulse). The probe laser was directly from the first OPA and all pump wavelengths except 199.7 nm were generated with the second OPA in two different ways, depending on the wavelength. For wavelengths in the range of 237.7–255.8 nm (0.5–0.8 μJ per pulse), the direct output of the second OPA was used. For shorter wavelengths (217.5–231.8 nm, 0.3–0.5 μJ per pulse), the output of this OPA in the range of 476–552 nm (>50 μJ per pulse) was mixed with a 400 nm laser beam (~80 μJ per pulse) using a β-BBO crystal (0.15 mm), which itself was the doubling of a fraction (~300 μJ per pulse) of the fundamental using another β-BBO crystal (0.1 mm). The wavelength of 199.7 nm (~0.1 μJ per pulse) was generated by frequency doubling, tripling, and then quadrupling the fundamental by using a series of β-BBO crystals. UV pulses were combined collinearly on a dichroic mirror without further compression, and then focused using an f/75 lens into the interaction region of the VMI spectrometer to intersect a seeded 2,4-DMP molecular beam. Time delays between pump and probe pulses were scanned using a computer-controlled stepper motor, which was located upstream of the first OPA to change the delay of the input fundamental.

The 2,4-DMP beam was generated by bubbling He of 4.0 bar through a liquid 2,4-DMP sample (Adamas, ≥98%) at room temperature using an Even-Lavie pulsed valve operated at 1 kHz. The 2,4-DMP molecular beam entered into the interaction chamber of the VMI spectrometer through a 1 mm skimmer (Beam Dynamics, Model 1). The pump pulse excited the 2,4-DMP molecules from their ground state to one or more electronically excited states by one-photon absorption, whereupon the delayed probe pulse produced photoelectrons *via* one-photon ionization. Photoelectron images arising from the pump or the probe laser alone were also recorded. The sum of the single color photo-electron images was subtracted in order to correct for back-ground photoelectrons generated from single color multiphoton

ionizations. The molecular beam condition was checked to make sure that the photoelectron signal from 2,4-DMP dimers or larger clusters was negligible. Pump–probe time delays were scanned back and forth multiple times to minimize any small hysteresis effects, and effects caused by the fluctuations and drifts in the laser pulse energies, pointing and molecular beam intensity, *etc.* The 2D photoelectron images were transferred to the 3D distributions using the basis-set expansion method.[28] The time-dependent photoelectron 3D distributions were further integrated along the recoiling angle to derive the kinetic energy distributions of the photoelectron, *i.e.*, time-resolved photoelectron spectroscopy (TRPES) spectra. Electron kinetic energy calibration was achieved using multi-photon ionization of Xe atoms. The cross-correlation (*i.e.*, instrumental response function (IRF)) between the pump and probe laser pulses was measured using two-color 1 + 1′ photoelectron spectra of nitric oxide, except for the longest pump wavelength of 255.8 nm. At the pump wavelength of 255.8 nm, the 1 + 1′ pump–probe energy is below the ionization potential of the NO molecule. The delay-dependent curve of the electron yield was fitted, based on the approximation that both pump and probe laser pulses have a Gaussian profile. The derived cross-correlations are 172 ± 3 (250.0 nm), 170 ± 4 (246.0 nm), 170 ± 4 (242.0 nm), 167 ± 8 (237.7 nm), 163 ± 10 (231.8 nm), 147 ± 4 (224.8 nm), 161 ± 3 fs (217.5 nm) and 166 ± 6 fs (199.7 nm). The error bars of the cross-correlation represent one standard deviation derived from the fit of the total electron yield to a Gaussian distribution. The time-zero overlap was also checked before and after the TRPEI measurement to make sure that there was no significant time-zero shift during the measurement.

In addition, the UV absorption spectrum of 2,4-DMP was measured under saturated vapor conditions using a commercial UV-visible spectrometer (Jasco, V-650), as shown in Fig. 1.

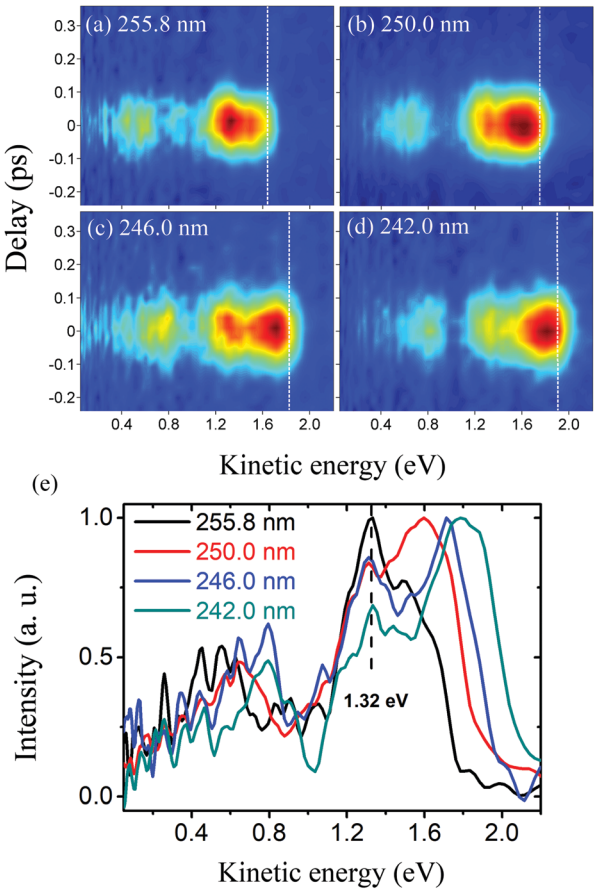

Fig. 2 (a–d) TRPES spectra of 2,4-DMP at pump wavelengths of 255.8, 250.0, 246.0 and 242.0 nm, respectively. The background photoelectrons generated from single color multiphoton ionization are subtracted. The photoelectron kinetic energy limits for ionization to the ground state of the cation are indicated by the white dashed lines. (e) The photoelectron kinetic energy distributions derived by integrating the TRPES spectra shown in (a–d) over all delays.

III Results and discussion

At longer pump wavelengths

The TRPES spectra of 2,4-DMP at pump wavelengths of 255.8, 250.0, 246.0 and 242.0 nm are shown in Fig. 2(a–d). At all these pump wavelengths, the photoelectron spectra are very similar to each other, extending over almost all the energetically allowed range, but mainly dominated by a strong, broad feature close to the corresponding energetic limit. The delay dependence of the photoelectron signal shows an extremely fast decay, with no observable dynamics at any photoelectron kinetic energy. By integrating the TRPES spectra at all delays, the photoelectron kinetic energy distributions are derived, which are plotted and compared with each other in Fig. 2(e). It is clear that the whole photoelectron spectra, especially the dominating broad feature close to the energetic limit, are shifted toward higher kinetic energy with a decrease of the pump wavelength, except for the feature at 1.32 eV which stays invariant. The amount of shift is close to the change in the pump photon energy. This observation might suggest that photoelectrons at 1.32 eV and other kinetic energies are generated from two different processes. At these pump wavelengths, the only energetically accessible electronic state is the $S_1(^1\pi\sigma^*)$ state. Therefore, these observations suggest the following scenario: the 1.32 eV peak is associated with the $S_1(^1\pi\sigma^*)$ state and photoelectrons at other kinetic energies are mainly from 1 + 1′ two color non-resonant ionization of 2,4-DMP. When the absorption to the electronically excited state is very weak, the TRPES spectrum could be dominated by the non-resonant two color ionization for an unfavorable photoionization case, as demonstrated recently by Townsend and coworkers in the first electronically excited state ($A_2(^1 3s/\pi\sigma^*)$) of pyrrole.[24] There are two more factors in support of the assignment of the 1.32 eV peak to the $S_1(^1\pi\sigma^*)$ state: (1) the $S_1(^1\pi\sigma^*)$ state is dominated by the 3s Rydberg character at the Franck–Condon (FC) region, and as such it may be expected to possess a minimum energy geometry very close to that of the D_0 state of the cation, resulting in the photoionization process being dominated by diagonal FC factors ($\Delta\nu = 0$). Therefore, a single peak is expected, as observed for the $A_2(^1\pi\sigma^*)$ state of NMP in the previous work.[22] (2) Since $\Delta\nu = 0$ FC factors dominate in the ionization process, the vibrational energy of the $S_1(^1\pi\sigma^*)$ state

deposited in the pump process will be conserved in the cation upon photoionization. The photoelectron kinetic energy (T_{ke}) will not vary with the change of the pump wavelength and it can be calculated with the following equation,

$$T_{ke} = h\nu_{probe} - (IP - A) \quad (1)$$

where $h\nu_{probe}$, IP and A represent the probe photon energy, the ionization potential of 2,4-DMP and the adiabatic excitation energy of the $S_1(^1\pi\sigma^*)$ state, and are 4.33 eV (286.5 nm), 7.54 eV,[29] and 4.54 eV (the longest photolysis wavelength at which a measurable H atom yield was obtained was 273.373 nm in the work by Ashfold and coworkers),[13] respectively. From eqn (1), a photoelectron kinetic energy of 1.33 eV is derived, which is in excellent agreement with the experimental observation.

By integrating the TRPES spectra over a narrow kinetic energy range (from 1.27 to 1.37 eV is used here), the photoelectron transients of the 1.32 eV feature are derived, as shown in Fig. 3. As alluded to by visual inspection, these photoelectron transients show an extremely fast decay. The lifetimes of the $S_1(^1\pi\sigma^*)$ state at these pump wavelengths can be estimated by fitting these photoelectron transients with an exponential decay function convoluted with the corresponding IRF. Lifetimes of 22, 11 and 29 fs are derived for 250.0, 246.0 and 242.0 nm, respectively. At 255.8 nm, these was no independently measured IRF available and no fit was done. But the photoelectron transient is very similar to those at the other three pump wavelengths and a similar lifetime is expected. These derived lifetimes are less than 20% of the corresponding IRFs and large uncertainties are expected. Therefore, we here estimate $\tau_{\pi\sigma^*} < 30$ fs for the decay of the $S_1(^1\pi\sigma^*)$ state.

These experimental results are consistent with those from the study by Stavros and coworkers[16] in which the time-resolved total H-atom product yield was measured. The appearance time of the H-atom product from the $S_1(^1\pi\sigma^*)$ state was determined to be about 120 fs and varied little with the pump wavelength in the range of 272–238 nm. The time constants derived in the current study are clearly much shorter than those derived in the time-resolved total H-atom product yield experiment. This underlines the fact that while the time constants derived from the total H-atom product yield experiment are the times needed to completely break the N–H bond and form the H atom product, those derived in the current experiment are only the times for the wave packet escaping out of the ionization window to a geometry with a much extended N–H bond on the potential energy surface of the $S_1(^1\pi\sigma^*)$ state. Therefore, they are supposed to be shorter.

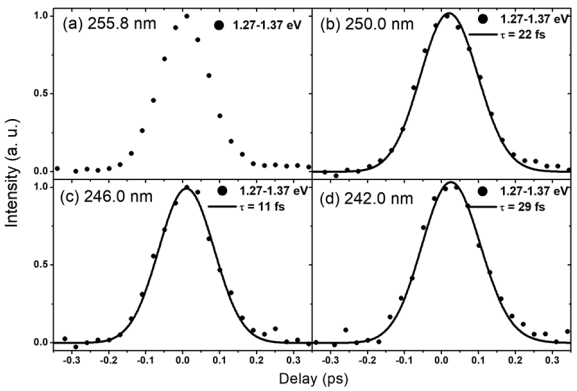

Fig. 3 Normalized photoelectron transients at 1.32 eV for pump wavelengths of 255.8 (a), 250.0 (b), 246.0 (c) and 242.0 nm (d), respectively. The solid circles show the experimental data, while the solid lines show the fits to the photoelectron transient with an exponential decay function convoluted with the corresponding IRF. No fit is done for the pump wavelength of 255.8 nm due to the lack of an independently measured IRF at this pump wavelength.

There is one thing worthy of note. In the data analysis of the time-resolved total H-atom product yield, a sharp rise and decay feature at $\Delta t = 0$ with a decay time constant much less than the IRF was observed, which was attributed by the authors as multiphoton dissociative ionization.[16] It was hard to analyze whether this multiphoton dissociative ionization channel has an electronic state of a very short lifetime as an intermediate resonance or not. The current experiment suggests that there should be a certain contribution from non-resonant multiphoton dissociative ionization in which no electronic state was involved as an intermediate resonant state. This contribution is associated with a zero time constant and is hard to distinguish from the resonant contribution with a time constant much shorter than the IRF. In the current study, the $1 + 1'$ two photon non-resonant ionization dominates the photoelectron signal. It would be infeasible to isolate the minor contribution associated with the $S_1(^1\pi\sigma^*)$ state from the dominating non-resonant photoelectron background in the total ion/electron yield experiments, highlighting the importance of differentially analyzing the photoelectron with respect to the kinetic energy, with techniques such as TRPEI.

At shorter pump wavelengths

The TRPES spectra of 2,4-DMP at pump wavelengths of 231.8, 224.8, 217.5 and 199.7 nm are shown in Fig. 4(a–d). At all these four pump wavelengths, the photoelectron spectra are dominated by a strong, narrow peak at 2.0 eV. The contribution from photoelectrons at lower kinetic energies (below 1.8 eV) is very small at 231.8 nm, but increases rapidly with a decrease in the pump wavelength. At 199.7 nm, another peak around 2.6 eV appears. The delay dependence of the photoelectron signal shows a fast decay, but is obviously slower than those at longer pump wavelengths discussed in the previous section. In order to extract more detailed information from these TRPES data, a 2D global least-squares method was employed to simultaneously fit data at all time delays and photoelectron kinetic energies. A single exponential decay function convoluted with the corresponding IRFs was used and satisfactory fits were derived. The photoelectron kinetic energy distributions derived from the fit are shown in Fig. 4(e). The derived time constants are 66 ± 10, 63 ± 13, 58 ± 8 and 63 ± 9 fs for pump wavelengths of 231.8, 224.8, 217.5 and 199.7 nm, respectively. In the data analysis, time-zeros were varied in the range of the time-zero drifts experimentally measured and the cross-correlations were also varied in the range of their uncertainties to obtain a best fit (minimum χ^2). This analysis also served to estimate the confidence intervals of these time constants.

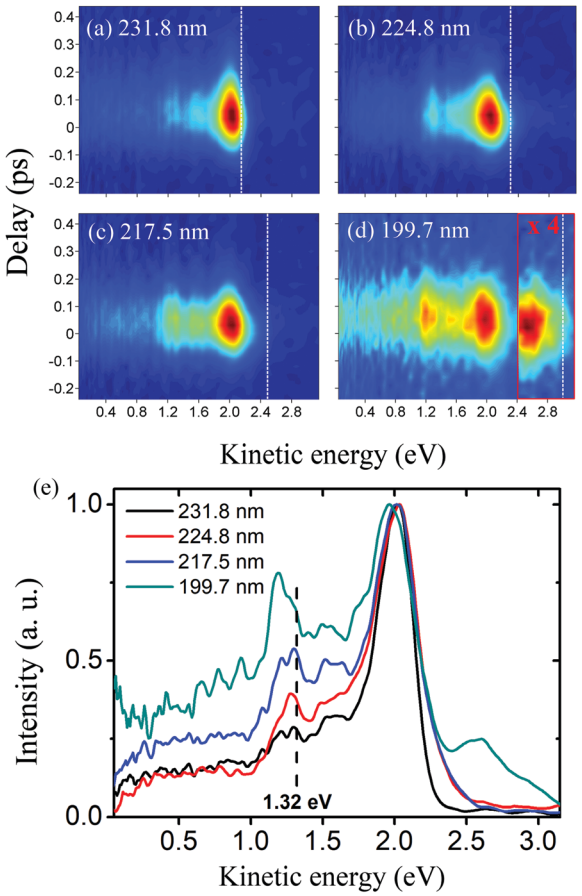

Fig. 4 (a–d) TRPES spectra of 2,4-DMP at pump wavelengths of 231.8, 224.8, 217.5 and 199.7 nm, respectively. The background photoelectrons generated from single color multiphoton ionization are subtracted. The photoelectron kinetic energy limits for ionization to the ground state of the cation are indicated by the white dashed lines. (e) The photoelectron kinetic energy distributions derived from the 2D global least-squares fit to the data.

The photoelectron kinetic energy distribution and its dependence on the pump wavelength are better presented in Fig. 4(e): the strong, narrow peak at 2.0 eV stays invariant with the change of the pump wavelength, while the feature below 1.8 eV increases rapidly with a decrease of the pump wavelength, with the detailed kinetic energy distributions being very similar for all four pump wavelengths. The TRPES spectra at these shorter pump wavelengths show differences with those at longer pump wavelengths in both their photoelectron kinetic energy distributions and the associated time constants, suggesting that different electronic state(s) other than $S_1(^1\pi\sigma^*)$ should be involved. This is also consistent with the UV absorption spectrum in which a fast rise appears around a wavelength of 240 nm, suggesting the onset of much stronger transition(s) to another electronic state(s). There is no assignment of the UV absorption spectrum of 2,4-DMP available. By analogous assignment compared to the UV absorption spectrum of pyrrole, the broad, strong absorption band in the wavelength range of 240–200 nm, especially the long wavelength part of this band, should be dominated by transitions to the states of Rydberg character, mainly the $^1\pi$3p Rydberg states and the $S_2(^1\pi\sigma^*)$ state.[17,30] These states are highly mixed in their electronic characters and strong intensity borrowing effects are present. At the short wavelength end of this band, electric dipole-allowed transitions to the $^1\pi\pi^*$ states start to contribute and become dominating at even shorter wavelengths. The 2.0 eV peak and the feature below 1.8 eV are present in the whole wavelength range of 231.8–199.7 nm, with the latter becoming increasingly important with a decrease of the pump wavelength. Therefore, it is very unlikely that the $^1\pi\pi^*$ states are responsible for the main features observed at these pump wavelengths and the components observed should be associated with the lower-lying Rydberg states. In the next section, it will be shown that the $S_2(^1\pi\sigma^*)$ state is observed at a pump wavelength of 237.7 nm, with a lifetime of 130 fs. Therefore, we tentatively assign the components observed at these shorter pump wavelengths to the $^1\pi$3p Rydberg states. The analysis of the photoelectron angular distributions (see ESI†) provides no solid information about the electronic character(s) of the excited state(s) involved, but does suggest that the excited state(s) involved at these pump wavelengths should be the same and they decay independently. Further theoretical calculations, including the simulation of the UV absorption spectrum, wave packet propagation, and photoionization cross section calculations, are needed to unambiguously identify the electronic states involved. In the photoelectron kinetic energy distribution at 199.7 nm, there is another weak peak at 2.6 eV showing a similar decay time constant. This might be associated with one of the $^1\pi\pi^*$ states, transition to which starts to appear around 200 nm.

The current TRPES spectra provide very little information on the decay channels of the electronic states involved. However, the 1.32 eV peak appears again in the photoelectron kinetic energy distribution at each of these pump wavelengths (indicated by a dashed black vertical line in Fig. 4(e)), suggesting that internal conversion to the $S_1(^1\pi\sigma^*)$ state might be one of the decay channels. However, due to the extremely fast decay of the $S_1(^1\pi\sigma^*)$ state, no solid evidence for this assignment can be extracted from the current experimental data. It is also likely that the decay to the $S_1(^1\pi\sigma^*)$ state only represents one of the decay channels for these electronic states. There might be some other decay channels which could not be seen in the current experiment. One of the candidates is the decay to the ground state directly from these states. This channel is not detectable in the current experiment since one probe photon is not enough to ionize the ground state 2,4-DMP directly.

In summary, we propose that 2,4-DMP is mainly excited to the $^1\pi$3p Rydberg states at the pump wavelength range of 231.8–199.7 nm. These states decay independently with a similar time constant of about 60 fs. Further experimental and theoretical studies are clearly needed to validate these assignments.

At a pump wavelength of 237.7 nm

Besides the pump wavelengths discussed above, the TRPES spectrum was also measured at a wavelength between the longer and shorter pump wavelengths, 237.7 nm, as shown in Fig. 5(a). This TRPES spectrum bears certain similarities with those at other pump wavelengths, especially those at shorter pump

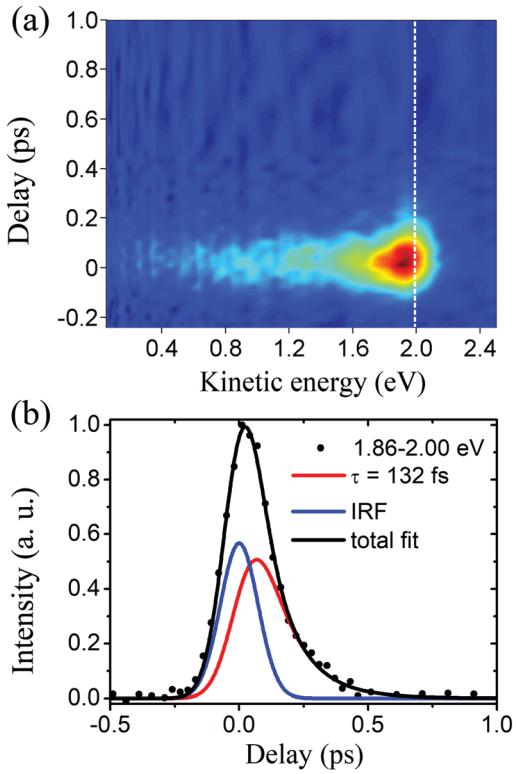

Fig. 5 (a) TRPES spectrum of 2,4-DMP at pump wavelengths of 237.7 nm. The background photoelectrons generated from single color multiphoton ionization are subtracted. The photoelectron kinetic energy limit for ionization to the ground state of the cation is indicated by the white dashed line. (b) Normalized photoelectron transient in the kinetic energy range of 1.86–2.00 eV. The solid circles show the experimental data, while black, blue and red lines show the total fit, the non-resonant photoionization and photoionization from the $^1\pi\sigma^*$ state contributions to the total fit, respectively.

wavelengths. The photoelectron extends over the whole kinetic range with a strong and broad peak close to the energetic limit. At this pump wavelength, contributions are expected both from $1 + 1'$ non-resonant photoionization, which dominates the TRPES spectra at longer pump wavelengths, and from the $^1\pi3p$ Rydberg states, which dominate the TRPES spectra at 231.8 nm. However, there is a weak, narrow peak at 1.93 eV worth noting. This 1.93 eV peak decays with a time constant of about 100 fs and is present in neither longer nor shorter pump wavelength TRPES spectra. The second $^1\pi\sigma^*$ state is located around this energetic position. Similar to the $S_1(^1\pi\sigma^*)$ state, this state is also dominated by the 3s Rydberg character at the FC region and a single sharp peak is expected in the photoionization spectrum. This is consistent with this 1.93 eV peak in the TRPES spectrum at 237.7 nm. With the photoelectron kinetic energy of 1.93 eV, the adiabatic excitation energy of this $^1\pi\sigma^*$ state can be calculated using eqn (1) and a number of 5.14 eV is returned. This adiabatic excitation energy of the $^1\pi\sigma^*$ state is 0.6 eV higher than that of the $S_1(^1\pi\sigma^*)$ state, in very good agreement with the vertical excitation energy difference calculated by Ashfold and coworkers,[13] providing further support to the assignment of this 1.93 eV peak. The photoelectron transient at 1.93 eV is fitted with a model including an exponential decay function convoluted with the IRF and an IRF to account for contributions from this $^1\pi\sigma^*$ state and the non-resonant photoionization, respectively (Fig. 5(b)). The fit quality was satisfactory and a lifetime of 132 ± 23 fs was derived.

Methyl substitution effects on the excited-state dynamics of pyrrole

Comparisons of the experimental results for 2,4-DMP with those for pyrrole and NMP provide some detailed insights into the methyl substitution effects on the excited-state dynamics of pyrrole. Here, we only focus on the lowest $S_1(\pi\sigma^*)$ state for which a most complete data set is available from our works and other previous studies. At 242 nm and shorter photoexcitation wavelengths, lifetimes less than 50 fs have been reported for the $S_1(\pi\sigma^*)$ state of pyrrole.[12,14,21] At 250 nm, a more than twice longer lifetime (126 fs) was reported.[14] This was attributed to the small barrier along the C–N dissociation coordinate and the population in the FC region has to escape *via* tunneling. The lifetimes (<30 fs) derived in the current study for the $S_1(\pi\sigma^*)$ state of 2,4-DMP are virtually the same as those for pyrrole at similar photoexcitation wavelengths. Stavros and coworkers have reported time constants of around 120 fs for the N–H bond dissociation along the repulsive $S_1(\pi\sigma^*)$ state surface of 2,4-DMP and these time constants are invariant with the photoexcitation wavelengths in the range of 276–238 nm.[16] These N–H bond dissociation time constants for 2,4-DMP are similar to that for pyrrole at a photoexcitation wavelength of 250 nm, but longer than those for pyrrole at shorter photoexcitation wavelengths. For NMP, a dramatic difference was observed: the lifetime of the $S_1(\pi\sigma^*)$ state is around one to three orders of magnitude larger than that for pyrrole.[22,23] This was explained to be due to an increased barrier along the C–N dissociation coordinate.

The adiabatic $S_1(\pi\sigma^*)$ state surface corresponds to the lower adiabat formed through an avoiding–crossing between the bound diabatic $^1\pi3s$ Rydberg and the repulsive $^1\pi\sigma^*$ valence states.[1,2] A barrier is developed along the N–H (N–CH_3 for NMP) dissociation coordinate.[2] The 3s Rydberg character is associated with the N atom and the σ^* character is mainly localized along the N–H (N–CH_3 for NMP) bond. For methyl substitution on the pyrrole ring positions (such as in 2,4-DMP), both the 3s and the σ^* orbitals should be only barely affected and the energetic position and topology of the $S_1(\pi\sigma^*)$ state surface should be untouched, causing large similarities between pyrrole and 2,4-DMP. The methyl substitution at the N atom position, however, should result in relatively large changes in the σ^* orbital. For the case of NMP, an increased barrier along the C–N dissociation coordinate is rendered. At the same time, the much larger mass of the CH_3 group inhibits any short-time tunneling through this barrier. Therefore, the lifetime of the $S_1(\pi\sigma^*)$ state of NMP becomes orders of magnitude longer and intersystem crossing to a lower triplet state was suggested as the main decay mechanism.[23]

IV Conclusions

The dynamics of 2,4-DMP following excitation at wavelengths in the range of 255.8–199.7 nm were studied with the TRPEI technique.

We conclude that excitation at longer wavelengths (255.8, 250.0, 246.0 and 242.0 nm) results in population of the $S_1(^1\pi\sigma^*)$ state, which decays out of the photoionization window with a time constant of less than 30 fs. At 237.7 nm, the second $^1\pi\sigma^*$ state is excited, which decays in 132 fs. At shorter pump wavelengths (231.8, 224.8, 217.5 and 199.7 nm), the assignments are less clear-cut. We tentatively assign the transitions to the $^1\pi3p$ Rydberg states, having a similar lifetime of about 60 fs. These lifetimes vary little with the pump wavelength in the range of 213.8–199.7 nm. Internal conversion to the $S_1(^1\pi\sigma^*)$ state seems to be one of the decay channels.

Conflicts of interest

There are no conflicts to declare.

Acknowledgements

This work was supported by the National Natural Science Foundation of China (21573228), the National Basic Research Program of China (973 Program, 2013CB922202) and the Ministry of Science and Technology of China (2012YQ12004704). The authors are grateful to Dr Simon Neville (University of Ottawa) for helpful discussions.

References

1 A. L. Sobolewski and W. Domcke, *Chem. Phys.*, 2000, **259**, 181–191.
2 A. L. Sobolewski, W. Domcke, C. Dedonder-Lardeux and C. Jouvet, *Phys. Chem. Chem. Phys.*, 2002, **4**, 1093–1100.
3 M. N. R. Ashfold, B. Cronin, A. L. Devine, R. N. Dixon and M. G. D. Nix, *Science*, 2006, **312**, 1637–1640.
4 M. N. R. Ashfold, G. A. King, D. Murdock, M. G. D. Nix, T. A. A. Oliver and A. G. Sage, *Phys. Chem. Chem. Phys.*, 2010, **12**, 1218–1238.
5 G. M. Roberts, D. J. Hadden, L. T. Bergendahl, A. M. Wenge, S. J. Harris, T. N. V. Karsili, M. N. R. Ashfold, M. J. Paterson and V. G. Stavros, *Chem. Sci.*, 2013, **4**, 993–1001.
6 G. M. Roberts and V. G. Stavros, *Chem. Sci.*, 2014, **5**, 1698–1722.
7 D. A. Blank, S. W. North and Y. T. Lee, *Chem. Phys.*, 1994, **187**, 35–47.
8 J. Wan, J. Meller, M. Hada, M. Ehara and H. Nakatsuji, *J. Chem. Phys.*, 2000, **113**, 7853–7866.
9 J. Wei, A. Kuczmann, J. Riedel, F. Renth and F. Temps, *Phys. Chem. Chem. Phys.*, 2003, **5**, 315–320.
10 B. Cronin, M. G. D. Nix, R. H. Qadiri and M. N. R. Ashfold, *Phys. Chem. Chem. Phys.*, 2004, **6**, 5031–5041.
11 H. Lippert, H. H. Ritze, I. V. Hertel and W. Radloff, *ChemPhysChem*, 2004, **5**, 1423–1427.
12 R. Montero, A. Peralta Conde, V. Ovejas, M. Fernandez-Fernandez, F. Castano, J. R. Vazquez de Aldana and A. Longarte, *J. Chem. Phys.*, 2012, **137**, 064317.
13 T. N. V. Karsili, B. Marchetti, R. Moca and M. N. R. Ashfold, *J. Phys. Chem. A*, 2013, **117**, 12067–12074.
14 G. M. Roberts, C. A. Williams, H. Yu, A. S. Chatterley, J. D. Young, S. Ullrich and V. G. Stavros, *Faraday Discuss.*, 2013, **163**, 95–116.
15 R. Montero, V. Ovejas, M. Fernández-Fernández, Á. P. Conde and A. Longarte, *J. Chem. Phys.*, 2014, **141**, 014303.
16 M. Staniforth, J. D. Young, D. R. Cole, T. N. V. Karsili, M. N. R. Ashfold and V. G. Stavros, *J. Phys. Chem. A*, 2014, **118**, 10909–10918.
17 S. P. Neville and G. A. Worth, *J. Chem. Phys.*, 2014, **140**, 034317.
18 V. Ovejas, R. Montero, M. Fernández-Fernández and A. Longarte, *J. Phys. Chem. A*, 2015, **119**, 3355–3365.
19 D. V. Makhov, K. Saita, T. J. Martinez and D. V. Shalashilin, *Phys. Chem. Chem. Phys.*, 2015, **17**, 3316–3325.
20 M. Sapunar, A. Ponzi, S. Chaiwongwattana, M. Malis, A. Prlj, P. Decleva and N. Doslic, *Phys. Chem. Chem. Phys.*, 2015, **17**, 19012–19020.
21 G. Wu, S. P. Neville, O. Schalk, T. Sekikawa, M. N. R. Ashfold, G. A. Worth and A. Stolow, *J. Chem. Phys.*, 2015, **142**, 074302.
22 G. Wu, S. P. Neville, O. Schalk, T. Sekikawa, M. N. R. Ashfold, G. A. Worth and A. Stolow, *J. Chem. Phys.*, 2016, **144**, 014309.
23 L. Blancafort, V. Ovejas, R. Montero, M. Fernández-Fernández and A. Longarte, *J. Phys. Chem. Lett.*, 2016, **7**, 1231–1237.
24 S. W. Crane, M. M. Zawadzki, J. O. F. Thompson, N. Kotsina, O. Ghafur and D. Townsend, *J. Chem. Phys.*, 2016, **145**, 234304.
25 M. Barbatti and K. Sen, *Int. J. Quantum Chem.*, 2016, **116**, 762–771.
26 N. C. Cole-Filipiak, M. Staniforth, N. D. N. Rodrigues, Y. Peperstraete and V. G. Stavros, *J. Phys. Chem. A*, 2017, **121**, 969–976.
27 Z. He, Z. Chen, D. Yang, D. Dai, G. Wu and X. Yang, *Chin. J. Chem. Phys.*, 2017, **30**, 247–252.
28 V. Dribinski, A. Ossadtchi, V. A. Mandelshtam and H. Reisler, *Rev. Sci. Instrum.*, 2002, **73**, 2634–2642.
29 V. K. Potapov and O. A. Yuzhakov, *Dokl. Akad. Nauk SSSR*, 1970, **192**, 131.
30 S. Neville, *private communication*, 2017.

